

Geometric Interpretation of Sensitivity to Structured Uncertainties in Spintronic Networks

S. P. O’Neil^{1,*}, E. A. Jonckheere², S. Schirmer³

Abstract—We present a geometric model of the differential sensitivity of the fidelity error for state transfer in a spintronic network based on the relationship between a set of matrix operators. We show an explicit dependence of the differential sensitivity on the fidelity (error), and we further demonstrate that this dependence does not require a trade-off between the fidelity and sensitivity. Rather, we prove that for closed systems, ideal performance in the sense of perfect state transfer is both necessary and sufficient for optimal robustness in terms of vanishing sensitivity. We demonstrate the utility of this geometric interpretation of the sensitivity by applying the model to explain the sensitivity versus fidelity error data in two examples.

I. INTRODUCTION

Exploiting the unique properties of quantum systems has the potential to revolutionize applications in communications, sensing, and computing [1], [2]. However, harnessing any technological “quantum advantage” requires external controls that not only meet exacting performance criteria, but retain a high level of performance in the face of model uncertainty. While classical H_∞ synthesis methods with guaranteed performance margins are applicable to a subset of open quantum systems undergoing weak continuous measurement [3], [4], such methods are ill-suited to the marginally stable dynamics of closed quantum systems such as idealized spintronic networks. As such, post-synthesis selection of acceptable controllers based on an assessment of the robustness or the sensitivity of the performance measure is common. Various methods for delivering such assessments can be found in the literature, ranging from stochastic [5], [6] to analytic [7], [8], [9].

Previous work has applied robustness assessments across a range of controllers to determine whether a trade-off between performance and robustness is a fundamental limitation in quantum control problems. Such a trade-off might be expected from the fundamental limitation of classical feedback control, encapsulated by the frequency domain identity $S + T = I$, where S and T represent the error and log-sensitivity, resp. In [9], we showed that there is a trade-off between performance and robustness in the time domain in the sense

¹ Department of Electrical Engineering & Computer Science, United States Military Academy, NY, USA. sean.oneil@westpoint.edu

² Dept of Electrical & Computer Engineering, University of Southern California, CA, USA. jonckhee@usc.edu

³ Faculty of Science & Engineering, Physics, Swansea University, UK. s.m.shermer@gmail.com

that the normalized logarithmic sensitivity of the fidelity error diverges as the error approaches zero. However, both [8] and [10] suggest that such a trade-off does not necessarily hold for suboptimal controllers for closed systems, in that the best-performing controllers (lowest fidelity error) are not necessarily those with the worst robustness (magnitude of the log-sensitivity). Furthermore, [11] provided examples of state transfer in spintronic networks where controllers with the best fidelity exhibited the smallest unnormalized differential sensitivity to parameter variations. Similarly, the results of [12] indicated a high concordance between the fidelity error and differential sensitivity for gate control problems, indicating that the best performing controllers are also the most robust.

The purpose of this paper is to investigate why such differing trends between error and sensitivity exist for state transfer problems. We develop a geometric interpretation of the differential sensitivity of the fidelity error to parametric uncertainty and use it to derive an explicit relationship between the magnitude of the sensitivity and the fidelity of transfer. The established relationship shows that there need not be a trade-off between the sensitivity and fidelity error and provides insight into the most important factors that determine the magnitude of the sensitivity. As part of the exposition, we provide necessary and sufficient conditions for vanishing sensitivity. Finally, we analyze two case studies to demonstrate the utility of the derived sensitivity model.

II. PRELIMINARIES

A. Physical Model and Control Problem

As in [10], we consider a coupled network of N spin-1/2 particles with $2^N \times 2^N$ real Hamiltonian

$$H_{\text{tot}} := \sum_{m \neq n} J_{nm} (X_n X_m + Y_n Y_m + \kappa Z_n Z_m). \quad (1)$$

J_{mn} is the coupling strength between spin m and n and $\{X_n, Y_n, Z_n\}$ is the respective Pauli operator acting on spin n , formally the N -fold tensor product of $(n-1)$ copies of the 2×2 identity matrix with a Pauli matrix $\{\sigma_x, \sigma_y, \sigma_z\}$ in the n th position. We consider the case of uniform coupling with $J_{mn} = J$ for all pairs (m, n) . We restrict the dynamics to the single excitation subspace (SES), the subspace of the Hilbert space isomorphic to \mathbb{C}^{2^N} corresponding to a single excited spin in the network. This is justified when the goal is

to transfer the state of the system from that of a single excited "input" spin to a single excited "output" spin with all other spins in the ground state, tantamount to transfer of a single qubit of information. While control of quantum systems in an open-loop manner via optimally shaped time-varying fields is a mainstay in quantum control [1], we consider the alternative paradigm of shaping the energy landscape of a closed system to facilitate the desired evolution [13], [14]. In the interest of model simplicity, we introduce time-invariant external fields to maximize the probability of state transfer from a given pure input state $|\psi_0\rangle$ to a pure output state $|\psi_f\rangle$. As detailed in [15], these control fields enter the Hamiltonian as scalars Δ_n on the diagonal of the SES Hamiltonian. We also consider only XX coupling since in the SES any coupling terms generated by $\kappa Z_n Z_m$ are diagonal and can be absorbed into the Δ_n controls. In terms of the Schrödinger dynamics, we have the initial value problem

$$|\dot{\psi}(t)\rangle = -iH|\psi(t)\rangle, \quad |\psi(0)\rangle = |\psi_0\rangle, \quad (2)$$

where H is the controlled Hamiltonian in the SES and units are chosen such that $\hbar = 1$. The Δ_n are generated by maximizing the probability of transfer, or fidelity, at a read-out time t_f given by $F = |\langle\psi_f|\psi(t_f)\rangle|^2$. See [10], [15] for details on the controller synthesis problem.

B. Uncertainty Model

To analyze the robustness of the controlled system, we use an uncertainty model that enables evaluation of how the introduction of uncertainty or disturbances alters the performance metric. In line with previous work [8], [9], [16] we consider real parametric uncertainty to the Hamiltonian represented as

$$\tilde{H} = H + \delta_n f_n S_n. \quad (3)$$

H is the nominal controlled Hamiltonian, and δ_n represents a small, real perturbation strength. S_n is the structure associated with the uncertainty indexed by n . f_n is a factor that accounts for scaling by the control field strength for those n that index uncertainty in a control channel; otherwise (e.g., for uncertainty in the couplings) $f_n = 1$.

C. Bloch Formulation

To put the analysis in the framework of a real vector space, we use the Bloch formulation to describe the perturbed dynamics [17]. Consider the most general description of the Schrödinger dynamics where the density operator $\rho(t)$ for the pure state $|\psi(t)\rangle$ is given by $|\psi(t)\rangle\langle\psi(t)|$. The perturbed dynamics generated by (3) are given by the von-Neumann equation

$$\dot{\tilde{\rho}}(t) = -i[\tilde{H}, \tilde{\rho}(t)]. \quad (4)$$

Taking the adjoint representation of this equation with respect to an orthonormal basis $\{\sigma_n\}_{n=1}^{N^2}$ of the $N \times N$ Hermitian matrices, such as the generalized Gell-Mann basis [18],

yields the mapping $-i\tilde{H} \mapsto \text{ad}_{-iH} := \tilde{A} \in \mathbb{R}^{N^2 \times N^2}$ with elements

$$\tilde{A}_{mn} = \text{Tr}(-i\tilde{H}[\sigma_m, \sigma_n]), \quad (5)$$

where $[\cdot, \cdot]$ is the matrix commutator [17]. By linearity of the commutator and trace, $-iH \mapsto A \in \mathbb{R}^{N^2 \times N^2}$ and $-iS_n \mapsto S_n \in \mathbb{R}^{N^2 \times N^2}$ so that $\tilde{A} = A + \delta_n f_n S_n$. As $-iH$ and $-iS_n$ are skew-Hermitian, it follows from the expansion (5) that A and S_n are skew-symmetric. The state ρ maps to $r \in \mathbb{R}^{N^2}$ with elements $r_m = \text{Tr}(\rho\sigma_m)$ so that $\rho_0 \mapsto r_0 \in \mathbb{R}^{N^2}$, $\rho_f \mapsto r_f \in \mathbb{R}^{N^2}$, and the state equation is

$$\dot{r}(t) = \tilde{A}r(t), \quad r(0) = r_0 \quad (6)$$

with solution $\tilde{r}(t) = e^{\tilde{A}t} r_0$. The fidelity at the read-out time t_f is $F = r_f^T e^{\tilde{A}t_f} r_0$. The fidelity error is $e = 1 - F$. Finally, we define $\Phi := e^{\tilde{A}t_f}$ as the state transition matrix at t_f and nominal A and define its perturbed counterpart as $\tilde{\Phi}$.

D. Differential Sensitivity

With this framework, the un-normalized differential sensitivity of e to a perturbation structured as S_n is given by $\zeta_n := \partial e / \partial \delta_n$ [9], [19]. Given the spectral decomposition of A (at its nominal value), $A = M \Lambda M^\dagger$,

$$\begin{aligned} \zeta_n &= -t_f f_n r_f^T M \left(\int_0^1 e^{t_f \Lambda(1-s)} M^\dagger S_n M e^{t_f \Lambda s} ds \right) M^\dagger r_0 \\ &:= -t_f f_n u^T (Z_n \odot X) v \end{aligned} \quad (7)$$

where $Z_n = M^\dagger S_n M$, $u = M^\dagger r_f$, $v = M^\dagger r_0$, and \odot denotes the Hadamard product. Denoting $i\lambda_k$ as the k th diagonal element of Λ , the entries of X are

$$x_{k\ell} = \begin{cases} e^{i\lambda_k t_f}, & \lambda_k = \lambda_\ell \\ \frac{e^{i\lambda_k t_f} - e^{i\lambda_\ell t_f}}{it_f(\lambda_k - \lambda_\ell)}, & \lambda_k \neq \lambda_\ell \end{cases}. \quad (8)$$

Alternatively, we may define the operator K_n such that $r_f^T (K_n) r_0 := u^T (Z_n \odot X) v$ and

$$\zeta_n = -t_f f_n r_f^T (K_n) r_0. \quad (9)$$

III. GEOMETRIC INTERPRETATION OF THE SENSITIVITY

A. Derivation of the Model

We now establish an analytic dependence of ζ_n , the differential sensitivity to an uncertainty indexed by n , on the fidelity error e , or equivalently, the fidelity F . We take a geometric approach and consider the operators Φ and K_n as elements of $\mathcal{B}(\mathbb{R}^{N^2})$, the space of bounded operators on \mathbb{R}^{N^2} [20]. With the Hilbert-Schmidt inner product for $A, B \in \mathcal{B}(\mathbb{R}^{N^2})$, $\langle A, B \rangle = \text{Tr}(A^T B)$ with compatible definition of the norm $\|A\|$. The orthogonal projection of A in the direction of B is given by $\mathcal{P}_B(A) = \frac{1}{\|B\|^2} \langle A, B \rangle B$. Setting $\hat{B} = B/\|B\|$, we have $\mathcal{P}_B(A) = \langle A, \hat{B} \rangle \hat{B}$.

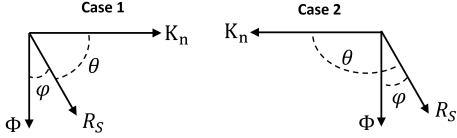


Fig. 1: Relation of operators in the subspace S_n .

Let S_n be the two-dimensional subspace of $\mathcal{B}(\mathbb{R}^{N^2})$ spanned by Φ and K_n .

Lemma 1: The operators Φ and K_n are orthogonal.

Proof: By definition of the inner product and the differential sensitivity, we have

$$\langle \Phi, K_n \rangle = \text{Tr} \left(e^{-t_f A} \left(\int_0^1 e^{t_f A(1-s)} S_n e^{t_f A s} ds \right) \right) \quad (10)$$

$$= \int_0^1 \text{Tr} (e^{-t_f A s} S_n e^{t_f A s}) ds = \text{Tr} (S_n). \quad (11)$$

Now (5) implies $S_n \in \mathfrak{so}(N^2)$, being real and skew-symmetric, so $\text{Tr}(S_n) = 0$ for any allowed structure S_n that retains unitary dynamics. ■

Define the operator $R \in \mathcal{B}(\mathbb{R}^{N^2})$ as $R = r_f r_0^T$. With this $F = \text{Tr}(R^T \Phi) = \langle R, \Phi \rangle$ and $-\zeta_n/(f_n t_f) = \text{Tr}(R^T K_n) = \langle R, K_n \rangle$, and the projection of R on the subspace S_n can be written as

$$\mathcal{P}_S(R) = \mathcal{P}_\Phi(R) + \mathcal{P}_{K_n}(R) := R_S. \quad (12)$$

The projection given in (12) is orthogonal as $\mathcal{P}_S^2 = \mathcal{P}_S$. Based on the projection definition, this is equivalent to

$$R_S = \frac{\langle R, \Phi \rangle}{N^2} \Phi + \frac{\langle R, K_n \rangle}{\|K_n\|^2} K_n = \frac{F}{N^2} \Phi + \frac{-\zeta_n}{f_n t_f \|K_n\|^2} K_n, \quad (13)$$

where $\|\Phi\| = N$ follows from $\Phi \in SO(N^2)$. Defining ϕ_n as the angle subtending R_S and Φ and θ_n as the angle subtending K_n and R_S gives

$$R_S = (\|R_S\| \cos \phi_n) \hat{\Phi} + (\|R_S\| \cos \theta_n) \hat{K}_n. \quad (14)$$

Figure 1 displays the relation of the operators in the subspace S_n . It follows that $F = N \|R_S\| \cos \phi_n$ and $\zeta_n = -t_f f_n \|K_n\| \cdot \|R_S\| \cos \theta_n$. By Lemma 1, we have that Φ and K_n are orthogonal so that either $\phi_n + \theta_n = \pi/2 \bmod \pi$ as in Case 1 or $|\phi_n - \theta_n| = \pi/2$ as illustrated in Case 2, and $\cos \theta_n = \pm \sin \phi_n$. Thus we have following relation between the magnitude of the differential sensitivity and the fidelity

$$|\zeta_n| = f_n t_f \|K_n\| \cdot \|R_S\| \cdot |\sin \phi_n| \quad (15a)$$

$$= f_n t_f \|K_n\| \cdot \|R_S\| \sqrt{1 - \left(\frac{F}{N \|R_S\|} \right)^2}. \quad (15b)$$

Eqs. (12)-(13) appear to be the quantum equivalent of the classical relation $S + T = I$, expressed in terms of the fidelity F rather than the error $e = 1 - F$. At the less conceptual level of (15b), holding $\|K_n\|$ and $\|R_S\|$ constant, $|\zeta_n|$ and e decrease simultaneously, in disagreement with the

classical limitations mandating a trade-off between error and sensitivity. What undermines the simplistic formulation that $|\zeta_n|$ and e are concordant is that $\|K_n\|$ and $\|R_S\|$ are not independent quantities; however, the first and crucial quantity can be bounded.

B. The Relation between $\|K_n\|$ and Eigenstructure

To determine how $\|K_n\|$ depends on the eigenstructure of the controller Φ , we employ (7), $K_n = M(Z_n \odot X) M^\dagger := M Q_n M^\dagger$. It follows immediately that $\|K_n\|^2 = \text{Tr} (Q_n^\dagger Q_n) = \sum_{k,\ell=1}^{N^2} |q_{k\ell}|^2$, and with (8)

$$q_{k\ell} = \begin{cases} z_{k\ell} e^{i \lambda_k t_f}, & \lambda_k = \lambda_\ell \\ z_{k\ell} \frac{e^{i \lambda_k t_f} - e^{i \lambda_\ell t_f}}{i t_f (\lambda_k - \lambda_\ell)}, & \text{otherwise} \end{cases} \quad (16)$$

so that

$$|q_{k\ell}|^2 = \begin{cases} |z_{k\ell}|^2, & \lambda_k = \lambda_\ell \\ |z_{k\ell}|^2 \text{sinc}^2 \left(\frac{1}{2} \omega_{k\ell} t_f \right), & \text{otherwise} \end{cases} \quad (17)$$

with the definition $\omega_{k\ell} := (\lambda_k - \lambda_\ell)$. We now identify the maximum of $\|K_n\|$ and establish strict positivity.

Lemma 2: $\|K_n\|$ is non-zero and bounded above by $\|S_n\|$.

Proof: To see that $\|K_n\|$ is not zero it suffices to show that $K_n^T K_n$ is never the zero matrix. Consider the integral expression of K_n from (9). Pulling $e^{A t_f} = \Phi$ out of K_n^T and K_n and using $\Phi^T \Phi = I$, we are left with $K_n^T K_n = \left(\int_0^1 e^{-t_f A s} S_n e^{t_f A s} ds \right)^T \left(\int_0^1 e^{-t_f A \tau} S_n e^{t_f A \tau} d\tau \right)$. Noting that $e^{\pm t_f A s} \in SO(N^2)$ and $S_n \in \mathfrak{so}(N^2)$, shows that the integrand is the adjoint action of the special orthogonal group on its Lie algebra for any s [21]. This Lie group conjugation is described by the mapping $\text{Ad}_{(e^{t_f A s})} : S_n \mapsto e^{-t_f A s} S_n e^{t_f A s}$. If the kernel of the integral of $\text{Ad}_{(e^{t_f A s})}$ is empty, it follows that $K_n^T K_n$ is not the zero matrix for non-trivial S_n . The spectrum of A given by $\{i\lambda_k\}_{k=1}^{N^2}$ determines the eigenvalues of $\text{Ad}_{(e^{t_f A s})}$, which are $e^{-i t_f (\lambda_k - \lambda_\ell) s}$ for k, ℓ indexed from 1 to N^2 . The eigenvalues of $\text{Ad}_{(e^{t_f A s})}$ retain the dependence of the integration variable s (equivalently τ), as can be verified by an explicit spectral decomposition of $\text{Ad}_{(e^{t_f A s})}$. Integrating s over the interval $[0, 1]$ yields eigenvalues for $\int_0^1 \text{Ad}_{(e^{t_f A s})} ds$ of 1 for $\lambda_\ell = \lambda_k$ and $i(1 - e^{-i(\lambda_k - \lambda_\ell)t_f})/(t_f(\lambda_k - \lambda_\ell))$ otherwise. As these eigenvalues are never zero, the kernel of the integral of $\text{Ad}_{(e^{t_f A s})}$ is empty. It follows that, for a non-trivial uncertainty structure S_n , $\|K_n\|$ is always non-zero. To establish the upper bound, note that when all sinc terms in (17) assume the maximum of 1, then $\|K_n\| \leq \sqrt{\sum_{k,\ell=1}^{N^2} |z_{k\ell}|^2} = \sqrt{\text{Tr} (M^\dagger S_n^\dagger M M^\dagger S_n M)} = \|S_n\|$. The upper bound of $\|S_n\|$ is only achieved if $\lambda_m = \lambda_n = \lambda$ for all pairs (m, n) , in which case, $\Phi = I e^{i \lambda t_f}$, which would provide a fidelity of zero for orthogonal states. ■

Replacing $\|K_n\|$ by its upper bound in (15a) yields an upper bound on $|\zeta_n|$, which decreases as ϵ decreases. But this behavior on the bound does not rule out an increase in $|\zeta_n|$ as ϵ decreases [9]. This indicates that any quantum performance limitation is not as straightforward as in classical control and that $|\zeta_n|$ and ϵ could be concordant [8], [10] or discordant [9].

C. Sufficient Condition for Vanishing Sensitivity

Lemma 3: For unitary evolution, the differential sensitivity ζ_n vanishes for any physically allowable perturbation if the controller Φ induces perfect state transfer.

Proof: As a physically realizable perturbation structure, S_n is Hermitian, and its Bloch representation S_n is skew-symmetric. For non-zero t_f and f_n , $-\zeta_n/(f_n t_f)$ is given by

$$\begin{aligned} \langle R, K_n \rangle &= \text{Tr} \left(R^T \left(\int_0^1 e^{t_f A(1-s)} S_n e^{t_f A s} ds \right) \right) \\ &= \text{Tr} \left(R^T \Phi \left(\int_0^1 e^{-t_f A s} S_n e^{t_f A s} ds \right) \right) = \text{Tr} \left(R^T \Phi W \right). \end{aligned}$$

From Lemma 2, the term in the integral is the adjoint action of $SO(N^2)$ on $\mathfrak{so}(N^2)$ for any value of s . Thus $W \in \mathfrak{so}(N^2)$, and $\langle R, K_n \rangle = 0$ is secured if the product $R^T \Phi$ is symmetric. We thus require $(r_f r_0^T)^T \Phi = r_0 r_f^T \Phi = (\Phi^T r_f) r_0^T$. Symmetry of this dyadic product requires $r_0 = \lambda \Phi^T r_f$ for some real λ . Since $\|r_f\| = \|r_0\| = 1$ and Φ is orthogonal, it follows that $\lambda = \pm 1$. For $\lambda = 1$, $r_f = \Phi r_0$, which is the condition for perfect state transfer from input state r_0 to r_f . Thus, for $\lambda = 1$, a controller inducing perfect state transfer is sufficient for $|\zeta_n| = 0$. For $\lambda = -1$, we would have $r_f = \Phi(-r_0)$. Observing that $(r_0)_m = \text{Tr}(\rho_0 \sigma_m)$ with $\rho_0 \geq 0$, it follows that $(-r_0)_m = \text{Tr}(-\rho_0 \sigma_m)$, and $(-r_0)$ would be associated with a nonpositive definite density, which is absurd. \blacksquare

D. Properties of R_S

The following observations demonstrate bounds on $\|R_S\|$.

Observation 1: At perfect state transfer $\|R_S\| = 1/N$ and $\cos \phi_n = 1$. This follows from Eq. (13) and the orthogonality of $\hat{\Phi}$ and \hat{K}_n , which implies $\|R_S\|^2 = (F/N)^2 + (\zeta_n/f_n t_f \|K_n\|)^2$. Lemma 3 shows that $\zeta_n = 0$ and thus $\|R_S\| = (1/N)$ for $F = 1$. The relation $F = N\|R_S\| \cos \phi_n$ further implies that $\cos \phi_n = 1$ for perfect state transfer.

Observation 2: For any fidelity, $\|R_S\|$ is bounded below by $\|R_S\| \geq F/N$. This follows directly from (15b), which requires $F/(N\|R_S\|) < 1$ for the sensitivity ζ_n to be real.

Though Observation 1 only provides the upper bound on $\|R_S\|$ in the exceptional case of perfect state transfer, we find that this holds as an upper bound in general. Fig. 2

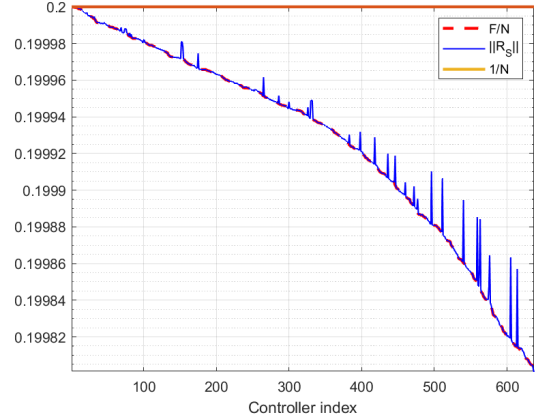


Fig. 2: Plot of $\|R_S\|$ and $1/F$ for a 5-ring and $|1\rangle \rightarrow |3\rangle$ transfer with coupling uncertainty indexed $n = 10$. Note that as the fidelity decreases $F/N \leq \|R_S\| \leq 1/N$.

for the case of a 5-ring and coupling uncertainty shows that $\|R_S\|$ remains below $1/N$ for all controllers.

In keeping with the geometric picture, we have $\|R_S\| = \cos \eta_n$ where η_n measures the minimum angle between R and any other elements of \mathcal{S}_n . We thus have $F = N \cos \eta_n \cos \phi_n$ and deduce that for a given uncertainty structure the magnitude of the sensitivity is given as $|\zeta_n| = t_f f_n \|K_n\| |\cos \eta_n| \cdot |\sin \phi_n|$.

IV. VANISHING DIFFERENTIAL SENSITIVITY

We now extend the result of [15, Th. 3] for sufficient conditions on vanishing sensitivity in spintronic networks. We use our geometric model to show that perfect state transfer is not only sufficient but necessary for vanishing sensitivity.

Theorem 1: For unitary evolution and controllers that yield non-zero fidelity, the differential sensitivity ζ_n vanishes for any physically allowable perturbation or uncertainty structure, if and only if the controller induces perfect state transfer.

Proof: Sufficiency is established by Lemma 3. For necessity, we refer to (15a). For any physically realizable controller, both f_n and t_f are non-zero. A non-trivial sensitivity thus requires non-zero $\|K_n\|$, $\|R_S\|$, and $\sin \phi_n$. From Lemma 2 we have the $\|K_n\|$ is always non-zero. From (13) it follows that the component of R_S in the $\hat{\Phi}$ direction is only zero if the fidelity is zero. So $\|R_S\| \neq 0$ unless the fidelity vanishes. Then $|\zeta_n| = 0$ requires $\sin \phi_n = 0$. But this is precisely the configuration of the operators in R_S for perfect state transfer. We thus conclude that the differential sensitivity vanishes if and only if the controller yields perfect state transfer. \blacksquare

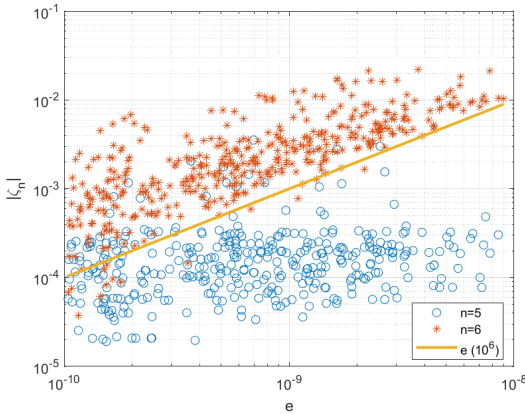


Fig. 3: Scatter plot of $|\zeta_n|$ versus e on a log-log scale for a $N = 4$, $|1\rangle \rightarrow |2\rangle$ transfer. The solid line indicates a line of unity slope on a log-log scale between e and $|\zeta_n|$

V. EXAMPLES

To demonstrate the utility of this model, we examine the fidelity error and sensitivity relationship for two state-transfer examples from taken from the data set in [10].

A. Differing Fidelity Error-Sensitivity Profiles

We begin with the case of state-transfer from spin 1 to spin 2 in a 4-ring with control mediated by static, time-invariant controls. We index the possible perturbations to the controls (i.e., perturbations to the diagonal elements of the SES Hamiltonian) by $n = 1$ though $n = 4$, and to the uncertainty in the couplings (i.e. uncertainty in the entries $((n-4), (n-3))$ and $((n-3), (n-4))$ of the SES Hamiltonian) by $n = 5$ though $n = 7$. Uncertainty to the entries $(1, 4)$ and $(4, 1)$ is indexed by $n = 8$. For all cases aside from $n = 5$ and $n = 7$, $\log e$ and $\log |\zeta_n|$ display a strong linear correlation with a Pearson r greater than 0.75. For the remaining two cases the correlation coefficient is less than 0.14. To investigate the origin of this differing behavior, we examine the differences between the $n = 5$ and $n = 6$ uncertainty cases as depicted in Figure 3. The strong linear relationship for the $n = 6$ case is borne-out by a Pearson r of 0.7503, while the much flatter trend for the $n = 5$ case can be verified by the Pearson r of 0.1373. We explain these different trends with the geometric model of Section III and (15a). Consider the visualization of the components of $|\zeta_n|/t_f$ shown in Figure 4. Note that both cases correspond to coupling uncertainty, so $f_n = 1$. For both cases, $\|\mathcal{R}_S\|$ is nearly constant at 0.25 across all controllers with a maximum deviation below this value on the order of 10^{-10} . This data is not displayed in Fig. 4. $\|\mathcal{K}_n\|$ shows some deviation across the controllers, however these deviations are unlikely to induce the different trends observed in Figure 3. In particular for $n = 5$, $\|\mathcal{K}_n\|$ has a mean of 3.650 and variance of 0.0759, while for $n = 6$ the statistics for $\|\mathcal{K}_n\|$ are 1.527 and 0.2752. However, as seen from Figure 4, the

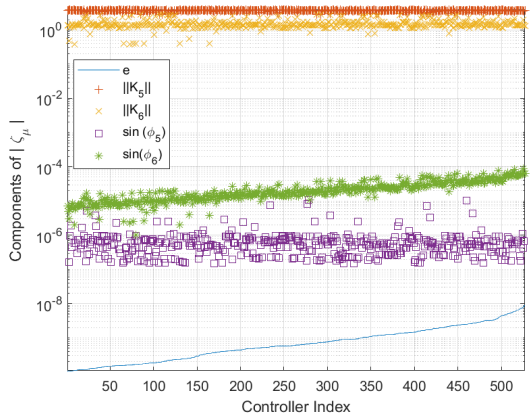


Fig. 4: Plot of components of $|\zeta_n|$ as depicted in Figure 3. Note that while variation in $\|\mathcal{K}_n\|$ is minimal, $\sin \phi_n$ trends positively with the fidelity error for $n = 6$ but shows a flat trend for $n = 5$.

TABLE I: Physical and geometric factors contributing to $|\zeta_5|$

Index	f_5	t_f	$\ \mathcal{K}_5\ $	$\ \mathcal{R}_S\ $	$\sin \phi_5$	$ \zeta_5 $
1585	2.35	198	1.71	0.199	1.48×10^{-7}	2.33×10^{-5}
1586	330	108	2.74	0.199	1.37×10^{-6}	2.69×10^{-2}
1587	17.0	400	1.68	0.198	4.50×10^{-5}	1.01×10^{-1}

behavior of $\sin \phi_n$ is markedly different for the controllers in the $n = 5$ versus $n = 6$ cases. The positive rank correlation between $\sin \phi_6$ and e is borne out by a Kendall τ of 0.8075. Conversely, the lack of rank correlation between metrics for the $n = 5$ case is evident in the weak Kendall τ of -0.0275.

This difference in behavior for $\sin \phi_n$ has the geometric interpretation that for the $n = 5$ structure, the change in the fidelity (error) is more attributable to the increase in the angle η_5 defining the inclination of \mathcal{R} with the subspace \mathcal{S}_5 than to an increase of ϕ_5 within the subspace. This minimal change of ϕ_5 with the fidelity error manifests as the absence of a clear trend between $|\zeta_5|$ and e as the fidelity error increases. Conversely, for the $n = 6$ case, an increase in the fidelity error is strongly correlated with, and nearly proportional to, an increase of the angle ϕ_6 within the subspace \mathcal{S}_6 . This suggests that those uncertainty structures that generate a subspace \mathcal{S}_n spanned by Φ and \mathcal{K}_n such that a change in the fidelity corresponds to a change in ϕ_n , are more sensitive (less robust) to variations in the fidelity error. To account for the read-out time t_f note that this is the same for both uncertainty cases and thus may be ruled out as the cause of the differing trends observed in Figure 3.

B. Large Variation in Sensitivity for Nearly Equal Error

We now study a case where there is no trend between $|\zeta_n|$ and e across controllers for the same uncertain parameter. We consider state transfer from spin 1 to spin 2 in a 5-ring with perturbation structure $n = 5$ (perturbation to the control addressing spin 5). Figure 5 depicts the sensitivity versus error profile, which does not reveal any visual trend between the two metrics. Rather, we see that the controllers

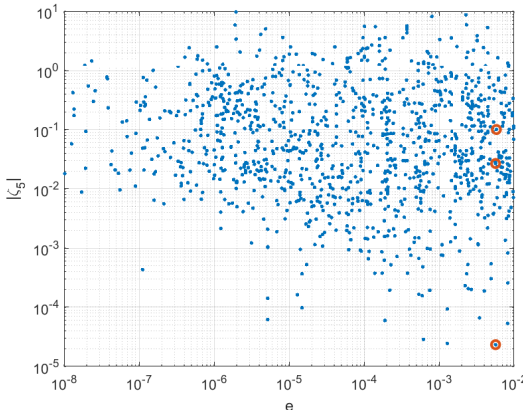


Fig. 5: Scatter plot of $|\zeta_5|$ versus e on a log-log scale for a $N = 5$, $|1\rangle \rightarrow |2\rangle$ transfer. The data points circled in red display widely varying sensitivity for nearly equal error.

with the lowest absolute value of sensitivity fall in the range of $10^{-4} < e < 10^{-2}$. We focus on the controller indices 1585, 1586, and 1587 (the red circled data points in Figure 5) which have an error in the range $5.67 \times 10^{-3} \pm 5 \times 10^{-5}$, while the differential sensitivity for these controllers spans orders of magnitude from 2.33×10^{-5} for controller 1585 up to 0.101 for controller 1587. We provide insight into this vast change in sensitivity by considering the geometric factors encoded in the size and orientation of the related matrix operators along with the physical parameters t_f and f_n as captured in (15a). Table I provides a summary of the relevant factors contributing to $|\zeta_5|$ for each controller. Referring to this data, we see that unlike in the previous example, the behavoir cannot be attributed simply to the effect of $\sin \phi_5$, but rather to a combination of the factors $\sin \phi_5$, t_f , and f_n . The extremely small sensitivity of controller 1585 is most attributable to a small angle ϕ_5 between Φ and R_S and small control amplitude. While controller 1586 demonstrates a $\sin \phi_5$ only an order of magnitude larger than the previous controller and a shorter read-out time, the large value of the control field contributes to an increase of over two orders of magnitude in $|\zeta_5|$. Finally, while controller 1587 admits a smaller control amplitude than its predecessor, the larger read-out time and $\sin \phi_5$, manifest as the largest sensitivity of the trio. This brief analysis justifies the premium placed on minimizing transfer times to increase robustness beyond the desire to minimize the impact of decoherence in open systems in general [22]. It also supports efforts to limit control amplitudes beyond energy considerations. Finally, while optimizing directly for small ϕ_n may not be possible, minimizing the fidelity error necessarily minimizes ϕ_n with a concomitant reduction in sensitivity.

VI. CONCLUSION

We developed a geometric model of the fidelity versus sensitivity to parametric uncertainty embodied in Eq. (12) more descriptive than the analytical formula (15b). We employed this model to provide insight into results of previous work

based on statistical analysis of the sensitivity versus fidelity error [8]. With this geometric model we expanded the scope of another previous work [15, Th. 3] by proving that perfect fidelity is not only sufficient, but necessary, for vanishing sensitivity. Future work should focus on relating R_S and ϕ_n to the eigenstructure of the controller in order to inform synthesis methods that account for these factors' impact on sensitivity.

REFERENCES

- [1] Christiane P. Koch *et al.*, “Quantum optimal control in quantum technologies. Strategic report on current status, visions and goals for research in Europe,” *EPJ Quantum Technology*, vol. 9, 7 2022.
- [2] Steffen J. Glaser *et al.*, “Training Schrödinger’s cat: quantum optimal control,” *EJP D*, vol. 69, 12 2015.
- [3] S. Wang, C. Ding, Q. Fang, and Y. Wang, “Quantum robust optimal control for linear complex quantum systems with uncertainties,” *IEEE Trans. Autom. Control*, vol. 68, no. 11, pp. 6967–6974, 2023.
- [4] M. R. James, H. I. Nurdin, and I. R. Petersen, “ H^∞ control of linear quantum stochastic systems,” *IEEE Trans. Autom. Control*, vol. 53, no. 8, pp. 1787–1803, 2008.
- [5] I. Khalid, C. A. Weidner, E. A. Jonckheere, S. G. Shermer, and F. C. Langbein, “Statistically characterizing robustness and fidelity of quantum controls and quantum control algorithms,” *Phys. Rev. A*, vol. 107, Mar. 2023.
- [6] A. Koswara, V. Bhutoria, and R. Chakrabarti, “Robust control of quantum dynamics under input and parameter uncertainty,” *Phys. Rev. A*, vol. 104, p. 053118, Nov 2021.
- [7] R. L. Kosut, M. D. Grace, and C. Brif, “Robust control of quantum gates via sequential convex programming,” *Phys. Rev. A*, vol. 88, nov 2013.
- [8] E. Jonckheere, S. Schirmer, and F. Langbein, “Jonckheere-Terpstra test for nonclassical error versus log-sensitivity relationship of quantum spin network controllers,” *Int. J. Robust Nonlinear Control*, vol. 28, p. 2383–2403, Jan. 2018.
- [9] S. O’Neil, S. Schirmer, F. C. Langbein, C. A. Weidner, and E. A. Jonckheere, “Time-domain sensitivity of the tracking error,” *IEEE Trans. Autom. Control*, vol. 69, no. 4, pp. 2340–2351, 2024.
- [10] S. P. O’Neil, F. C. Langbein, E. Jonckheere, and S. Shermer, “Robustness of energy landscape controllers for spin rings under coherent excitation transport,” *Research Directions: Quantum Technologies*, vol. 1, p. e12, 2023.
- [11] E. A. Jonckheere, S. G. Schirmer, and F. C. Langbein, “Structured singular value analysis for spintronics network information transfer control,” *IEEE Trans. Autom. Control*, vol. 62, no. 12, pp. 6568–6574, 2017.
- [12] S. O’Neil, C. Weidner, E. Jonckheere, F. Langbein, and S. Schirmer, “Robustness of dynamic quantum control: Differential sensitivity bounds,” *AVS Quantum Science*, vol. 6, no. 3, 2024.
- [13] A. Donovan, V. Beltrani, and H. A. Rabitz, “Quantum control by means of hamiltonian structure manipulation,” *Phys. Chem. Chem. Phys.*, vol. 13 16, pp. 7348–62, 2011.
- [14] R.-W. Zhang, C. Cui, R. Li, J. Duan, L. Li, Z.-M. Yu, and Y. Yao, “Predictable gate-field control of spin in altermagnets with spin-layer coupling,” *Phys. Rev. Lett.*, vol. 133, p. 056401, Aug 2024.
- [15] S. G. Schirmer, E. A. Jonckheere, and F. C. Langbein, “Design of feedback control laws for information transfer in spintronics networks,” *IEEE Trans. Autom. Control*, vol. 63, no. 8, pp. 2523–2536, 2018.
- [16] S. P. O’Neil, I. Khalid, A. A. Rompokos, C. A. Weidner, F. C. Langbein, S. Schirmer, and E. A. Jonckheere, “Analyzing and unifying robustness measures for excitation transfer control in spin networks,” *IEEE Control Syst. Lett.*, vol. 7, pp. 1783–1788, 2023.
- [17] F. F. Floether, P. de Fouquieres, and S. G. Schirmer, “Robust quantum gates for open systems via optimal control: Markovian versus non-Markovian dynamics,” *New J. Phys.*, vol. 14, p. 073023, jul 2012.
- [18] R. A. Bertlmann and P. Krammer, “Bloch vectors for qudits,” *J. Phys. A-Math.*, vol. 41, p. 235303, may 2008.
- [19] I. Najfeld and T. Havel, “Derivatives of the matrix exponential and their computation,” *Adv. Appl. Math.*, vol. 16, no. 3, pp. 321–375, 1995.

- [20] J. Siewert, “On orthogonal bases in the Hilbert-Schmidt space of matrices,” *J. Phys. Commun.*, vol. 6, p. 055014, May 2022.
- [21] D. Elliott, *Bilinear Control Systems: Matrices in Action*. Springer Publishing Company, Inc., 1st ed., 2009.
- [22] C. P. Koch, “Controlling open quantum systems: tools, achievements, and limitations,” *J. Condens. Matter Phys.*, vol. 28, p. 213001, 2016.